ELSEVIER

Computers & Geosciences 30 (2004) 429–443

COMPUTERS & GEOSCIENCES

www.elsevier.com/locate/cageo

Landslide hazard analysis for Hong Kong using landslide inventory and GIS

K.T. Chau*, Y.L. Sze, M.K. Fung, W.Y. Wong, E.L. Fong, L.C.P. Chan

Department of Civil and Structural Engineering, The Hong Kong Polytechnic University, Yuk Choi Road, Hung Hom, Kowloon, Hong Kong, China

Received 20 February 2002; accepted 5 August 2003

Abstract

This paper presents a landslide-inventory-based and GIS-based framework for systematic landslide hazard analysis by employing historical landslide data in Hong Kong, coupling with geological, geomorphological, population, climatic, and rainfall data. Based on 1448 landslide data from 1984 to 1998, the diurnal and seasonal distributions of landslides are established and compared with the seasonal rainfall variation. The cumulative fatalities and injuries caused by landslides increase with the cumulative rainfall in Hong Kong, indicating a strong correlation between rainfall and landslide consequences. The average annual fatality and injury rates in Hong Kong caused by landslide are 11.35 and 11.63, respectively. In terms of being hit by a landslide, squatter areas and roads on Hong Kong Island are at the highest risk. A frequency–volume relation for Hong Kong Island was established, and, using this relation, it was estimated that the return period of a 26,000 m^3 landslide (the size of 1995 Shum Wan Road Landslide) is about 3.12 years. A hazard zonation map for Hong Kong Island is established by using historical data. The potential use of GIS technology to incorporate various layers of information is illustrated using Hong Kong Island as an example. Both landslide hazard and risk maps are proposed using raster calculation.

Keywords: Natural terrain landslides; Data analysis; Hong Kong island; Hazard map; Geology

1. Introduction

Landslides can manifest themselves in many different forms, including rockfalls, rockslides, debris flows, soil slips, rock avalanches, and mud-flows. Some infrequent landslides may lead to catastrophes. For example, it was estimated that 200,000 people died in 1920 from an earthquake-induced loess flow in Kansu Province China (Hansen, 1984). More recently, 4000 people died after an earthquake-induced debris avalanche occurred at north peak of Nevados Huascaran, in Peru in 1962 (Hansen, 1984). Considering the scale of these events, they are basically unpreventable. The most reliable way to prevent landslide-induced casualties and economic losses is to avoid building towns or cities in the vicinity of steep terrains. But, this is considered impracticable or impossible in many countries due to the rapid growth of human population or due to the expensive cost in relocating of ancient or historical cities. Thus, regional landslide hazard analysis and management is becoming an important task for city planners and officials.

Landslide hazard and risk analysis for a town or city normally involves a sequence of mountain ranges surrounding the area, and thus the use of hazard map is found necessary. Landslide hazard map is very useful in estimating, managing and mitigating landslide hazard for a region (Anbalagan et al., 1993; Kienholz, 1978; PIARC, 1997). Many review articles have addressed the issue of landslide hazard and risk analysis and management. They include Leroi (1997), Hansen (1984), Fell

*Corresponding author. Tel.: +852-27666015; fax: +852-2334-6389.

E-mail address: cektchau@polyu.edu.hk (K.T. Chau).

0098-3004/$ - see front matter © 2004 Elsevier Ltd. All rights reserved.
doi:10.1016/j.cageo.2003.08.013

and Hartford (1997), Einstein (1988, 1997), Varnes (1984), and Hungr (1997). The scale of landslide hazard can be expressed in either regional basis, community basis or a site basis. When landslide hazard is estimated, we have to consider the historical records, the local geology (e.g. shallow or deep-seated landslides), lithology (e.g. physical and chemical behaviors of rocks and soils), structure (e.g. stratigraphic sequences, joint sets etc), geomorphology (e.g. steepness of slopes), hydrologic conditions (e.g. groundwater level), vegetation (e.g. form and type of vegetative cover), and climate (e.g. precipitation and temperature). The local stress condition is also an important factor that may relate to uplift, erosion, deposition, and groundwater fluctuation. We should also borne in mind that many of these parameters and conditions actually change with time.

Ideally, a reliable landslide hazard map should carry appropriate weights from historical landslide events, from geomorphological analysis, and from mechanics analysis of slides, falls, and flows of the earth mass. Since all three aspects of hazard analysis involve the handling and interpreting a large amount of factual, geological and simulated data, the use of computer or information technology is crucial to the success of such analysis. Since the mid 1980s, geographical information system (GIS) becomes a very popular technology used in calculating and managing natural hazards, including landslides (Coppock, 1995). Some of these GIS-based hazard analyses focus on earthquake-induced landslides (e.g. Luzi et al., 2000; Miles and Ho, 1999; Miles and Keefer, 1999; Refice and Capolongo, 2002), and some on hydrological-condition-induced landslides (e.g. Miller and Sias, 1998). GIS analysis has also been proposed to produce rockfall hazard map (e.g. Cancelli and Crosta, 1994). However, the reliability of the hazard analysis does not depend on which GIS software or platform we used but on what analysis method we employ (Carrara et al., 1999). Therefore, various methods of analysis have been proposed by many different authors (e.g. Dikau et al., 1996; Leroi, 1997; Guzzetti et al., 1999; Dai and Lee, 2002a, b; Carrara et al., 1999).

GIS technology has been used virtually everywhere in the world, including both developed and developing countries. For example, GIS technology has been applied to examine landslide hazard in North America: Los Angeles area, USA by Jibson et al. (2000), Glenwood-Springs, Colorado, USA by Mejianavarro et al. (1994), Moresby, Canada by Davis and Keller (1997), and Idaho, USA Gritzner et al. (2001); in South America: Manizales in Central Colombia by van Westen and Terlien (1996); in Asia: Jordan by Husein et al. (2000), Yongin, Korea by Lee and Min (2001), Bhagirathi Valley, Himalayas by Saha et al. (2002), Ramganga catchment, Himalayas by Gupta and Joshi (1990), Kulekhani watershed, Nepal by Dhakal et al. (1999), Phewa Tal watershed, Nepal by Rowbotham and Dudycha (1998), and Western Ghat, India by Nagarajan et al. (1998); in Europe: northern Spain by Duarte and Marquinez (2002), Tuscany, Italy by Luzi et al. (2000), Central Italy by Carrara et al. (1991), Southern Italy by Refice and Capolongo (2002), Fabriano, Italy by Luzi and Pergalani (1996), and Southeast England by Collison et al. (2000); and in Africa: Wondogenet area, Ethiopia by Temesgen et al. (2001).

In the case of Hong Kong, GIS-assisted landslide hazard analysis has only been proposed for Lantau Island, where the new International Airport is located (Dai et al., 2001, 2002; Dai and Lee, 2001b, 2002a, b; Lee et al., 2001). However, most of the population of Hong Kong does not locate at Lantau Island, but instead on the Hong Kong Island. Therefore, it is meaningful to consider the landslide hazard as well as the risk for Hong Kong Island, on which most of the tall buildings are located.

Therefore, the main objective of the present study is to consider more comprehensively the landslide hazard of Hong Kong, paying particular attention to Hong Kong Island and combining historical landslide data with GIS. In particular, diurnal and seasonal distributions of landslides are established. Correlation between rainfall and fatalities and injuries caused by landslides is examined. Facilities on Hong Kong Island at the highest risk are identified. The correlation between landslide occurrence and geological formation, slope angle, and slope height are investigated. A landslide hazard zonation map is also proposed based on spatial distribution of historical data. The potential use of GIS technology in incorporating geological, geomorphological, and climatic data is illustrated using Hong Kong Island. The present discussion of the use of GIS technology in the hazard analysis on Hong Kong Island should shed new light on the future works in this direction. More detailed hazard analysis will be presented in our forthcoming papers.

2. Introduction to the geological and climatic conditions for Hong Kong

Before we consider the landslide hazard, it is informative to briefly introduce the geological and climatic conditions of Hong Kong Island.

2.1. Geological conditions of Hong Kong Island

Hong Kong can be divided into three distinct areas: Hong Kong Island, Kowloon and the New Territories. The area of Hong Kong Island is 77.5 km^2, or about 7% of the total area 1098 km^2 of Hong Kong. The terrain of Hong Kong Island is hilly to mountainous with steep slopes exceeding 30°, covered by superficial deposits of

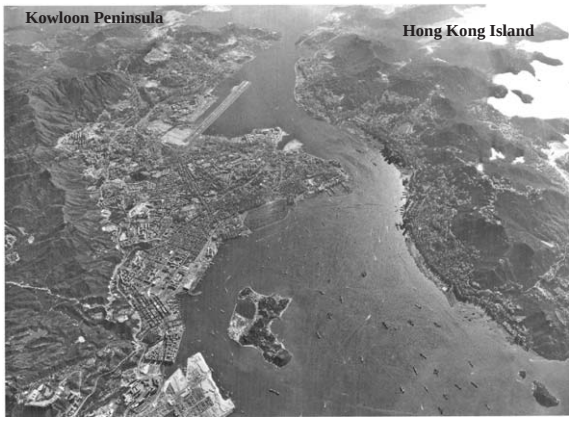

Fig. 1. Aerial photograph of Hong Kong Island and Kowloon Peninsula (after Fyfe et al., 2000).

Quaternary age. The highest point is the Victoria Peak at 554 m. Fig. 1 shows an aerial photograph of the hilly Hong Kong Island and Kowloon Peninsula. The location of the photograph in Hong Kong is shown in Fig. 2. Hong Kong Island is underlain mainly by volcanic rock and intrusive granite.

The granites are younger than the volcanic rocks, having been intruded in various stages into the volcanic rock mass about 170 million years ago. The volcanic rocks are mainly of Middle and Lower Jurassic age, and of variable type and composition, but consisting mainly of tuffs, and are frequently metamorphosed. In general, the outcropping rocks of Hong Kong are highly weathered, and a mantle of debris flow deposits covers the north-facing slopes of Victoria Peak. The deposits come almost entirely from the volcanic rocks around the Peak. In most places the average thickness of the deposits is about 2 m, but in some places the deposits may be up to 30 m. In addition, talus deposits have also been delineated at three locations of the north-facing slopes of Victoria Peak (Fyfe et al., 2000).

2.2. Climatic conditions of Hong Kong

Hong Kong's climate is sub-tropical, with a winter temperature of 10°C to summer temperature of exceeding 31°C. Foggy weather is expected from March to May, while a hot and humid weather with occasional showers and thunderstorms, and frequent typhoon visits from May to September. When a typhoon comes close to Hong Kong, rain can become heavy and widespread and last for a few days. Subsequent landslides are commonly observed.

The mean annual rainfall ranges from around 1300 mm along the coast to more than 3000 mm on mountains. About 80% of the rain falls between May and September; and the wettest month is August with an average monthly rainfall of about 400 mm.

3. Landslides hazard analysis based on landslide inventory

In this section, landslide data are used for hazard analysis. They are mainly extracted from the reports on "Hong Kong rainfall and landslides" which are published annually by the Geotechnical Engineering Office since 1984 and from a report compiling all landslide consequences since 1948 (GEO, 1996). Data before 1984 are incomplete since only landslides involving injuries and fatalities were included. The latest reports (1992–1996) seem to be much more complete than those reports before 1992. Also, the volume of landslides is missing in reports before 1992 and exact occurrence time is missing in many earlier entries. Note also that rockfall data has not been included in the present analysis since they have been analyzed by Chau et al. (1998, 2003). Another caution must be made is that most of the landslide records are for the failures of man-made slopes. For landslides on natural terrains, only those events leading to death, injury, or interruption of human activities have been included. For non-damaging natural terrain landslides, the locations of their occurrence must be close to human activities that caught the attention and caused concerns of the nearby residents, otherwise they will not be reported.

Fig. 3 shows some landslide events in Hong Kong. Fig. 3(a) shows the debris flows occurred on the natural terrain on Lantau Island in November 1996; Fig. 3(b) shows the Shun Wan Road landslide occurred on August 13, 1995, which involves a total of 26,000 m^3 of sliding mass and leads to 2 death and 5 injured; Fig. 3(c) shows the Po Shan Road landslide occurred on June 18, 1972, which leads to 67 deaths and severe damages to a 12-storey building; and finally Fig. 3(d) shows the Tsing Shan debris flow occurred on April 14, 2000.

Although it is very unlikely that the data compiled here are complete, this data set is considered reliable and should constitute a good basis for hazard analysis.

3.1. Diurnal and seasonal distributions for landslides in Hong Kong (1948–1996)

Diurnal rockfall frequency was established by Chau et al. (1998) for Hong Kong by using 129 data from 1949–1995. There is, however, no counterpart study for landslide data of Hong Kong. Therefore, Fig. 4 plots the diurnal landslide distribution by compiling a total of 623 data from 1948 to 1996. It appears that landslides often occur during daytime from 7 in the morning till 6 in the evening. The peak hour of landslide occurrence is at noontime. However, we should bear in mind that during

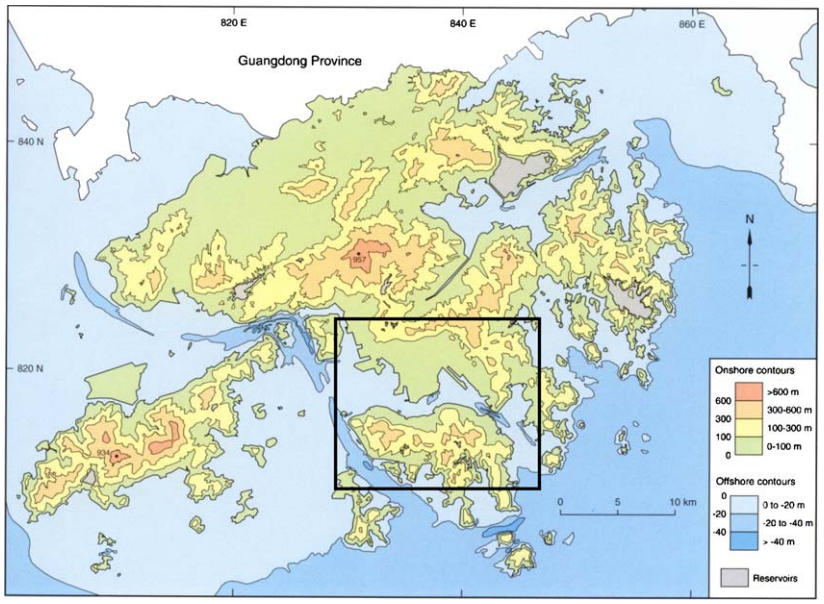

Fig. 2. Contour map of Hong Kong with coverage of photograph shown in Fig. 1 highlighted by a rectangle.

Fig. 3. Some landslides in Hong Kong: (a) debris flows on natural terrain of Lantau Island in November 1996; (b) Shun Wan Road landslide on August 13, 1995 with a total of 26,000 m^3 of sliding soil and leading to 2 dead and 5 injured; (c) Po Shan Road landslide on June 18, 1972 leading to 67 death and severe damages to a 12-storey building; and (d) Tsing Shan debris flow on April 14, 2000.

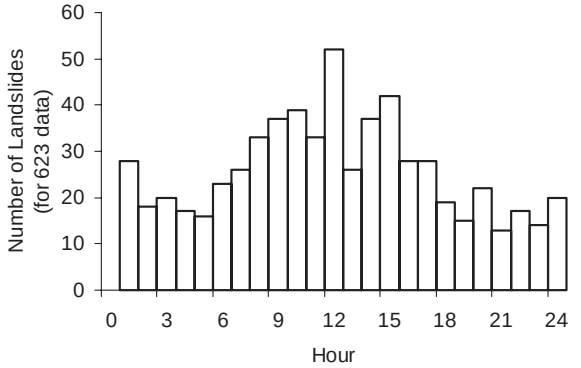

Fig. 4. Diurnal frequency of landslides in Hong Kong (1948–1996), and a total of 623 data have been used.

the daytime human activities are more active, thus the chance of spotting a landslide occurrence is higher than that during the nighttime. This conclusion is similar to that for the diurnal distribution for rockfall occurrence reported by Chau et al. (1998).

The seasonal distribution of rockfall events for Hong Kong has been considered by Chau et al. (1998). Fig. 5 plots the seasonal distribution for landslides occurred in Hong Kong Island together with the average daily rainfall and temperature. A total of 1448 data from 1984 to 1996 were plotted. Except for the month of May, the average monthly rainfall correlates very well with landslide occurrence. May has an abnormal high

frequency of landslides due to particular large number of entries from 1989 and 1992, making the average number of landslides greater than other months. To eliminate this abnormal effect, Fig. 6 plots the monthly variation of temperature, rainfall and landslides in the years of 1990 and 1991. The temperature, rainfall and number of landslides are given as solid circles, open circles and columns respectively. A very clear correlation between rainfall and landslide can now be observed.

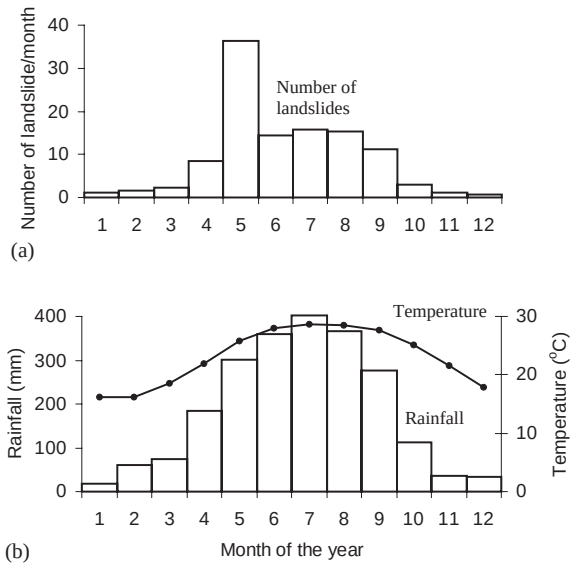

Fig. 5. (a) Seasonal variations of average landslide frequency in Hong Kong (1984–1996); and (b) seasonal distributions of rainfall (columns) and temperature (solid line with dots). Total number of landslide data used in the analysis is 1448.

3.2. Fatalities and injuries rate in Hong Kong (1948–1996)

The landslide caused casualties in Italy from 1410 to 1999 was estimated to be 12,421 deaths and injuries (Guzzetti, 2000); these casualties were caused by at least 996 landslides. This yields a casualty rate of 21 deaths and injuries per year in Italy span over a period of 590 years. Of course, the actual casualties should probably be higher than this value since the data set for landslides causing low casualty rate might have been incomplete before the 19th century. Similar landslide induced casualties for Hong Kong has not been done comprehensively. Therefore, Fig. 7 plots the cumulative number of fatalities and injuries caused by landslides from 1948 to 1996, together with the cumulative rainfall in meter for the same period. Total number of fatalities and injuries are 556 and 570, respectively. In summary, a total of 258 landslide events led to either death and/or injury, 117 of them killed 556 people. The average number of fatality per year is 11.35 and that for injury is 11.63. Incidentally, this figure tally to about 23 casualties per year which is comparable to those for Italy mentioned earlier. Considering the fact that the area of Italy is about 274 times of that of Hong Kong and the population is only 8.5 times of that of Hong Kong, the casualty rate per year per area induced by landslides are much higher in Hong Kong than in Italy. As mentioned earlier the figure for Hong Kong is only for landslides excluding rockfalls, while the Italian data include both rockfalls and landslides.

Estimating an average population of 4.12 millions from 1948 to 1996 (increased from 1.83 millions to 6.31 millions), the annual probability of death of an individual due to landslides in Hong Kong during this

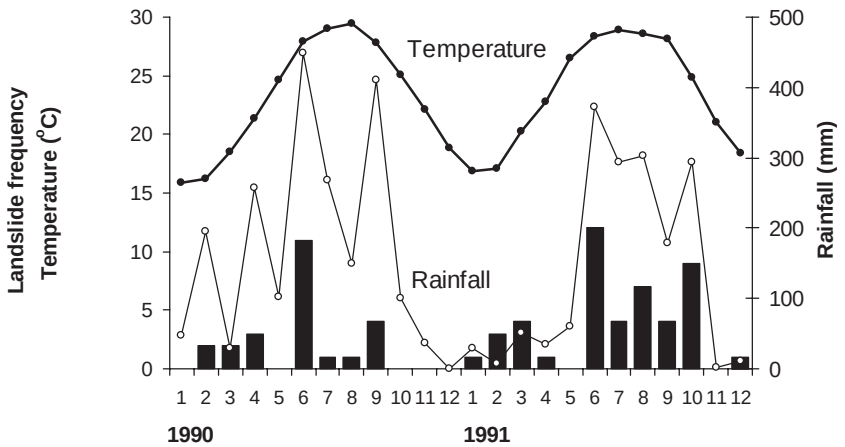

Fig. 6. Monthly variations of temperature, rainfall and its relation to landslides in 1990 and 1991. Average monthly temperatures are given in solid circles, while those for rainfall are in open circles. Number of landslides is given as columns. A total of 70 landslide data were used.

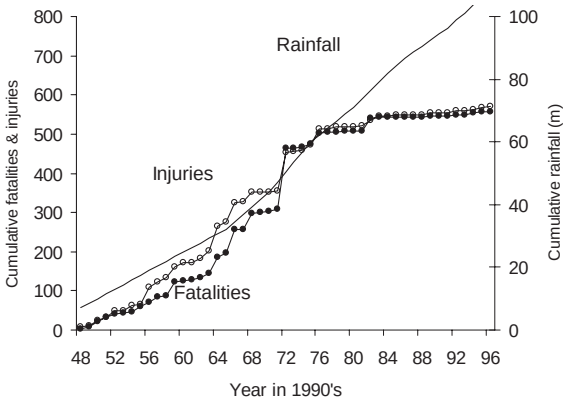

Fig. 7. Cumulative fatalities, injuries and rainfall in Hong Kong from 1948 to 1996. A total of 556 fatalities and 570 injuries were reported.

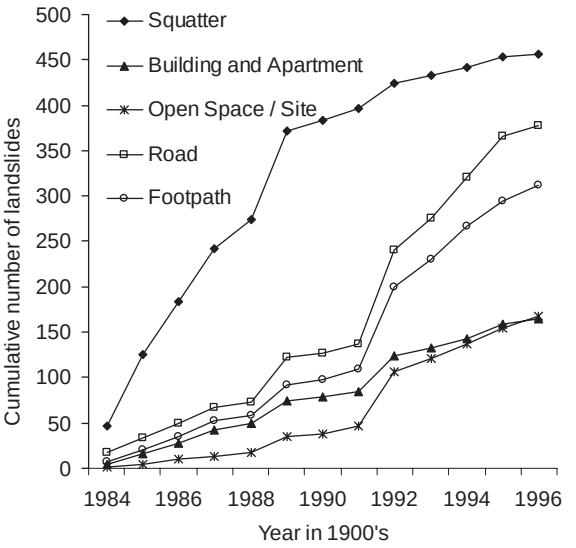

Fig. 8. Cumulative number of landslides affecting various facilities and utilities from 1984 to 1996, including squatter, road, footpath, open space/site, and building/apartment.

period is 0.00013 or an annual fatality rate of 2.75×10^{-6}, which is more than 10 times of the fatality rate caused by rockfall (Chau et al., 2003). Two particular incidents in 1972, Sau Mau Ping landslide (71 died and 60 injured) and Po Shan Road landslide (67 died and 20 injured), lead to the highest fatality and injury during that 49 year period (see the jumps in 1972 in Fig. 7). In recent years, the landslide preventive measure (LPM) program of the Geotechnical Engineering Office of Hong Kong government has been very successful; therefore, the average number of fatality and injury per year after 1972 drop to 3.88 and 4.83. In addition, on average every 100 mm of cumulative rainfall causes 0.79 dead and 0.79 injured from 1948 to 1996.

3.3. Landslide influence in Hong Kong (1948–1996)

It is of interest to know, at least statistically, where in Hong Kong or what kind of facilities is at a higher risk. Fig. 8 plots the cumulative number of events having influences on squatter (damage or evacuation), road (blockage or damage), footpath (blockage or damage), building (damage or evacuation), and open space (no direct influence) from 1984 to 1996. Note that some of these landslide events may affect more than one type of facilities; therefore, double count of influences is allowed in our analysis. As shown in Fig. 8, squatter areas in Hong Kong are at the highest risk, following by roads, pedestrian pavements or footpaths, and buildings. In recent years, landslide hazard on squatter is dropping while those for road and footpath is increasing. This is due to the rapid expansion of the highway system in Hong Kong in recent years and the gradual decrease of squatter areas because of public housing policy. In terms of probabilistic distributions, Fig. 9 shows that 28% of

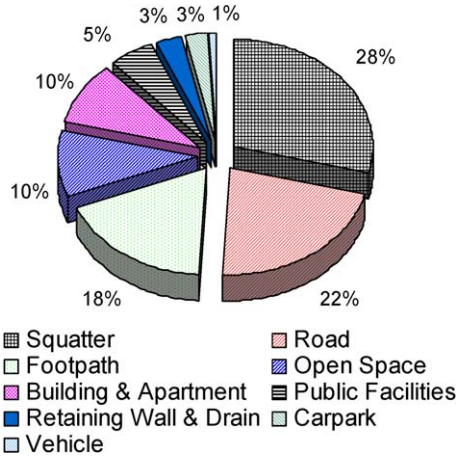

Fig. 9. Percentage distribution of landslides landing on squatter, road, footpath, open space, buildings, public facilities, retaining wall and drain, car park and vehicle.

landslides land on squatter areas, 22% on road, 18% on footpath, 10% on open space, 10% on buildings, 5% on public facilities, 3% on retaining walls and drains, 3% on car-parks and the remaining 1% on vehicles. The very low rate of direct hit on car suggests that the landslip warning system adopted by the Hong Kong Government during heavy rainfall has been effective in reducing fatality or injury on roads and highways.

3.4. Landslide hazard in different geological formations on Hong Kong Island (1992–1996)

It is of both theoretical and practical interest to investigate whether volcanic or igneous formation in Hong Kong is more conducive to landslide occurrence. Since there are clear differences in the joint spacing as well as in the rate of weathering occurring in tuff (the most common volcanic rock in Hong Kong) and granite (the most common igneous rock in Hong Kong), it is normally speculated that the rate of landslide occurrence should depend on the local geological formation. Therefore, in this study Hong Kong Island has been selected for such analysis. As shown in Fig. 10(a), about 64% of the surface geology of Hong Kong Island consists of volcanic formation, 28% of granitic formation while 8% of reclamation. A total of 312 landslide data with clear soil formation was used from 1992 to 1998 in the analysis, and the results are shown in the pie chart of Fig. 10(b). It was found that about 66% of the landslides occurred in soil originated from decomposed volcanic rocks, while 34% from granites. Considering the ratio of the area with surface geology of volcanic origin to that with granitic origin, there seems no strong correlation between landslide occurrence and geological formation. However, for the case of natural terrain landslides Evans et al. (1999) showed that landslides occurrences are strongly dependent on the geological formation.

3.5. Frequency and volume relation of landslides for Hong Kong Island

The frequency–volume relation for landslide in Hong Kong has been considered by Dai and Lee (2001a) from 1992 to 1997 by compiling a total of over 3000 data. In the present study, we attempt to establish a new

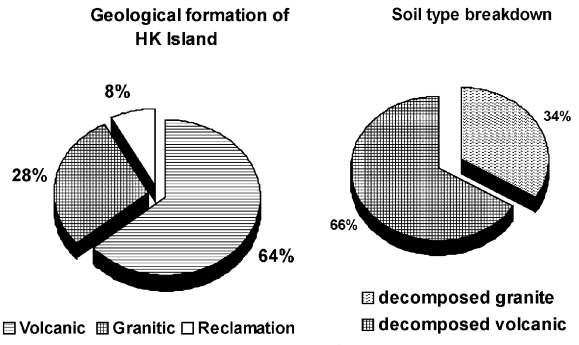

Fig. 10. Percentage distributions of: (a) geological formation and (b) landslide on soil types for Hong Kong Island. A total of 312 data with clear soil formation was used from 1992 to 1998 in analysis.

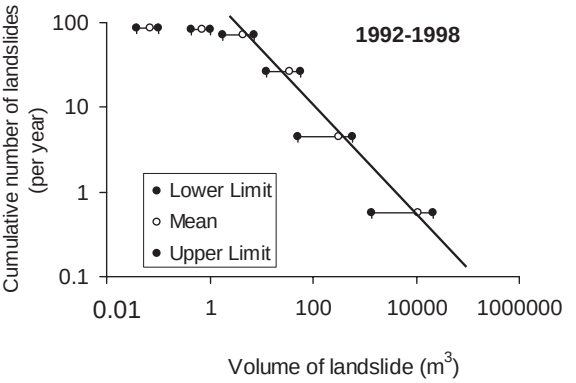

Fig. 11. Cumulative number of landslides per year versus volume of landslide for Hong Kong Island. A total of 594 data was used from 1992 to 1998 in analysis. Best fit line for larger event is also shown.

frequency–volume for Hong Kong Island because it is believed that the landslide data is much more complete for Hong Kong Island than for the whole Hong Kong. The population on Hong Kong Island is estimated to constitute 20% of the total population of Hong Kong while its area constitutes only 7% of the land of Hong Kong. Thus, the chance of not reporting a landslide event is probably 3 times lower than that of the rest of Hong Kong.

Fig. 11 plots the average cumulative number of landslides per year versus the volume of landslide for Hong Kong Island from 1992 to 1998. A total of 594 data was used from 1992 to 1998 in the analysis. Motivated by the study of Chau et al. (2003), the cell size is selected as logarithmic (i.e. 0.1–1, etc.). The average of the data within each logarithmic volume cell is plotted as an open circle, and lower and upper limits indicate "plus" or "minus" one standard deviation of the data within the same cell. Despite the fact that the data set for Hong Kong Island is of higher confidence comparing to the rest of Hong Kong, it is very unlikely that the data set for small events (say for volume of less than $5\,m^3$) is complete. Therefore, only the four larger data points in Fig. 11 are used in establishing the following self-similar frequency–volume relation, which is analogous to the Gutenberg–Richter relation for earthquake (Scholz, 1990; Chau et al., 2003):

$$\log_{10} N = a - b \log_{10} V, \tag{1}$$

where V and N are the volume of landslide and the cumulative number of landslide of scale V or larger for a specified period of time, and a and b are constants to be determined by data.

Based on the landslide data shown in Fig. 11, the following formula is established:

$$\log_{10} N = 2.3124 - 0.6357 \log_{10} V, \tag{2}$$

with a coefficient of correlation of 0.9968 (or $R^2 = 0.9936$). This simple relation can be used to estimate the return period of some larger events. For example, for a landslide of volume 26,000 m^3 (or the size of the 1995 Shum Wan Landslide shown in Fig. 3(b)) a return period of 3.12 years is expected. But, of course, the accuracy of this prediction depends on the completeness of our data set and the validity of the self-similar model proposed in (1).

3.6. Landslide hazard map for Hong Kong Island based on landslide inventory

One simple way to generate hazard map is the use of historical data or the inventory map, as proposed by Chau et al. (2003) for rockfall analysis. The pros and cons of such technique were discussed by Chau et al. (2003) and will not be repeated here. Inventory map of landslides has also been given for Umbria, Central Italy and used for geomorphological analysis by Cardinali et al. (2002). In the present study, the map of Hong Kong Island is first divided into square grids or cells of size of 500 m. A total of 921 landslide data from 1984 to 1996 are identified within the grids. The cumulative number of landslides within each cell is summed. Then contour lines are proposed based on the number of landslide per year within each cell; therefore 1 unit of contour line increment on these maps represents 1 landslide per 13 years per 0.25 km^2 (i.e. 1.23 landslide per year per square kilometer). Fig. 12(a) shows a typical plot of the landslide distribution together with the elevation contour plots (landslides and rockfall events are denoted by open and solid circles respectively), while Fig. 12(b) shows the hazard map for Hong Kong Island based on the analysis of historical data described above. In order to show more vividly the spatial distribution of the landslide occurrence, the contour plots shown in Fig. 12(b) is given with an uneven increment between the contour lines. In particular, the values of the six levels of contour lines shown in Fig. 12(b) are for 0.25, 0.75, 1.25, 2, 4, and 5 units in ascending order.

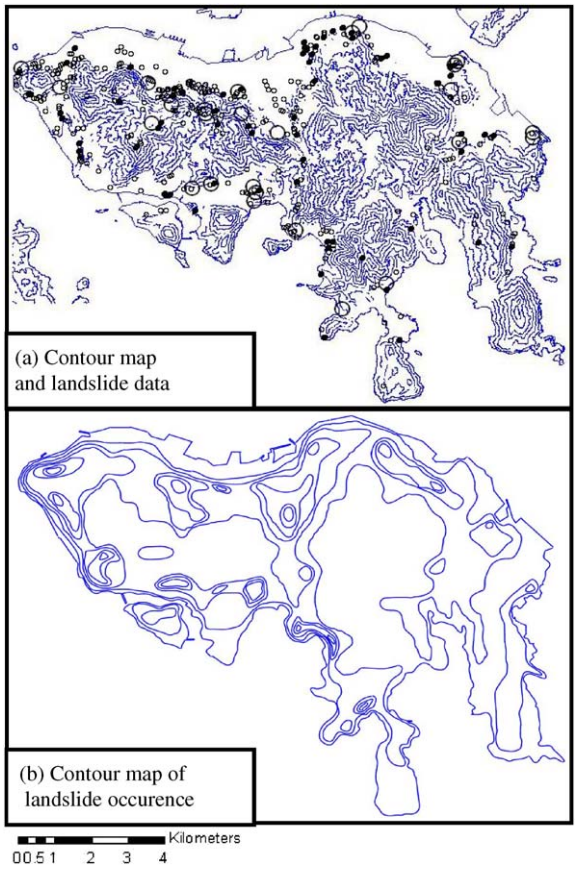

Fig. 12. (a) Spatial distribution of landslide data (solid and open circles are for rockfall and landslides respectively) with major landslides shown in bigger circles; (b) landslide hazard zonation map for Hong Kong Island based on historical record only. A total of 921 landslide data was used from 1984 to 1996. Values of six levels of contour lines are for 0.25, 0.75, 1.25, 2, 4, and 5 units and each unit corresponds to 1.23 landslide per km^2.

4. Use of GIS in analyzing landslide hazard

The limitation of the hazard map shown in Fig. 12 is that only landslide data has been used in generating the map. Clearly, a useful hazard zonation map should also depend on other factors that affect the occurrence and the mechanism of landslides such as, the local geology, geomorphology, lithology, hydrology, vegetation, and climate. Therefore, the next step is to incorporate these and other relevant parameters in our hazard analysis. In order to analyze landslide hazard systematically and efficiently, the use of a geographical information system (GIS) is essential (van Westen, 2000). The effect of the resolution of grid used in analyzes was discussed by Dhakal et al. (2000). Other hazard studies through the use of GIS include Lazzari and Salvaneschi (1999) and van Westen et al. (1999). Raster calculation adopted in GIS tremendously reduces the time of data analysis and provides the user a very powerful tool to examine the effects of various parameters.

4.1. Using GIS to examine correlation between landslides and slope data

Before we apply GIS to estimate landslide hazard by incorporating various factors, it is instructive to illustrate how we can use GIS to correlate landslide susceptibility in terms of various parameters. For example, Fig. 13 examines the correlations between

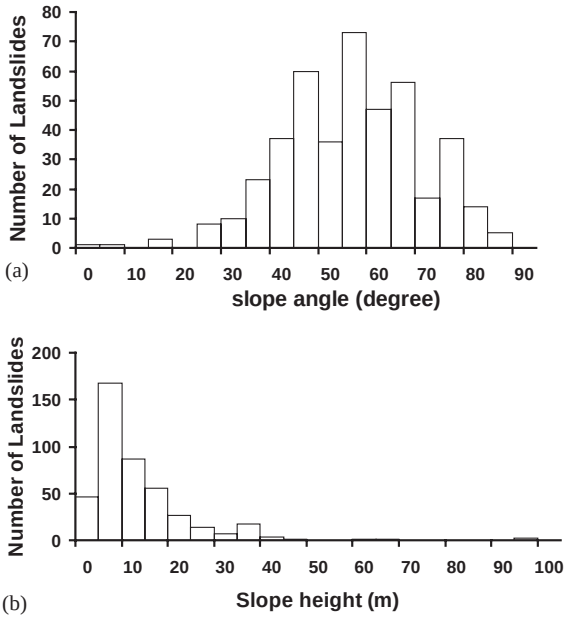

Fig. 13. Landslide distribution in terms of slope angle and slope height. A total of 428 data from Hong Kong Island has been used for analysis.

landslide occurrence and slope height and slope angle. In particular, using the "zonal statistics" available in the Spatial Analyst of ArcGIS 8.2 to generate correlation between any two layers of raster maps (say slope angle and landslide data in the present case), the landslide distributions in terms of slope angle and slope height are generated in Fig. 13 from a total of 429 landslide data of Hong Kong Island. The cell sizes for the slope angle and slope height are selected as 5° and 5 m respectively. For example, the number of landslides plotted within the cell labelled as 30° in Fig. 13(a) is the sum of those landslides with slope angle between 25° and 30° (i.e. $25^\circ \leqslant \theta < 30^\circ$, where θ is the slope angle). Fig. 13(a) shows that most of landslides occurred on a sloping ground of inclination from 55° to 60° and other landslide data distributed around this value in a form of normal distribution. Most landslides occurred at slopes with height of 5–10 m. These plots are useful for identifying the important parameters affecting landslide occurrence. Note, however, that landslide data used in the analysis for Fig. 13 are for cut-slope failures only, and natural terrain landslides are not included. For natural terrain landslides, Evans et al. (1999) have examined the correlations between landslide occurrence and degree of erosion, terrain landform, lithology, slope angle, slope aspect, elevation and vegetation for Hong Kong using aerial photographs and GIS.

4.2. Layers of information for multi-dimensional regression analysis

To yield a more reliable estimate of landslide hazard and risk, different layers of information must be incorporated into the GIS system. However, the way of selecting the important independent variables for landslide hazard analysis and the way of combining these variables are still under debate and is an area for further research. The main goal of the present section is not to discuss such method comprehensively, but to highlight the potential use of GIS technology through specific examples. ArcGIS 8.2 with Spatial Analyst was used for the present analysis.

Seven layers of information have been used in the present analysis, but of course many more layers can also be added to such hazard analysis as long as their correlations with landslide occurrences are clear and measurable. As summarized in the flowchart given in Fig. 14, terrain data (slope angle and elevation or referred as T1 and T2), environmental effect (rainfall or E1), geology information (soil deposit and lithology or G1 and G2), and landslide information (potential runout coverage and landslide inventory or L1 and L2) can be incorporated into hazard assessment using GIS. For example, for layer G2 (lithology or geological formations) tuff formation is more susceptible to natural terrain landslide occurrence than granitic formation (Evans et al., 1999). Thus, different hazard weightings may be assigned to different geological formations, and the same can also be applied to other layers. As shown in Fig. 14, all layer information has to be digitalized in GIS format and their correlation, expressed in hazard index, with landslide occurrence has to be established using the actual landslide data. Then, a multi-dimensional

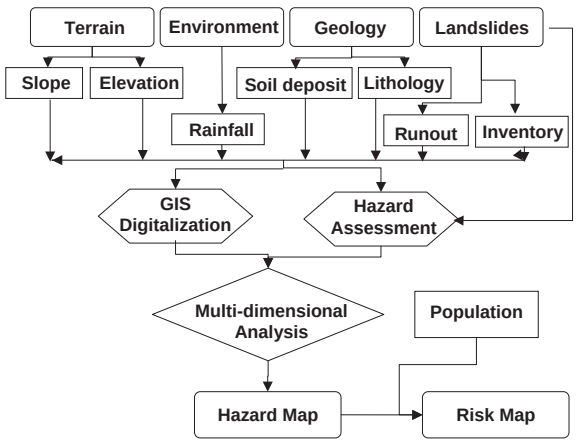

Fig. 14. Flowchart of landslide hazard and risk analyses based on GIS. In current study, only six levels of information were incorporated into hazard analysis and only population was included in risk analysis.

Table 1
Weightings and hazard indices for various categories, layers, and classes

Class No. (i)	Category	Layer (j)	Weighting (W_j)	Class (C_i)	Hazard index (H_{ji})
1	Terrain	Elevation (H)	0.5	0–200 m	0.9838
2				200–400 m	1.0000
3				400–600 m	0.9114
4		Slope angle (θ)	2.0	$<15^\circ$	0.0000
5				15–18°	0.0142
6				18–22°	0.0336
7				22–27°	0.1382
8				27–30°	0.2782
9				30–34°	0.5115
10				34–39°	1.000
11				39–45°	0.7164
12				$>45^\circ$	0.3300
13	Geology	Lithology	1.0	Rhyolitic tuff	1.0000
14				Trachytic tuff	0.5379
15				Fine-grain granite	0.3753
16				Medium-grain granite	0.3924
17				Tuff Breccia	0.5288
18				Coarse ash crystal tuff	0.6043
19				Quartz	0.2162
20				Granodiorite	0.2759
21		Soil deposit	1.0	Yes	1.0000
22				No	0.0000
23	Landslide	Past events	2.0	N (No. per 100 m^2)	$N/4$
24		Potential Runout	1.0	Yes	1.0000
25				No	0.0000
26	Environment	Rainfall	1.0	r (mm per month)	$r/1027$

analysis has to be used to yield the hazard map. In the present study, a risk map is also generated by considering the population distribution. The details are considered next.

4.3. Hazard analysis using raster calculation

Table 1 summarizes the weightings ($W_j, j = 1, 2, \ldots, 7$) and hazard indices (H_{ji}, $i = 1, 2, \ldots, 26$) that we have assigned to various layers. In the present study, all layer raster maps are normalized with respect to its maximum value such that the maximum possible value of the Hazard Index (H_{ji}) for each layer has been scaled to 1. In particular, the hazard indices for lithology, slope angle and elevation were derived from Tables 8, 10 and 12 of Evans et al. (1999) respectively. More specifically, the total number of landslide occurrence for each class of slope angle given in Table 10 of Evans et al. (1999) is normalized with respect to that of class 34–39° to yield the hazard index. The same procedure has been used to arrive at the first 20 hazard indices of Table 1. We speculate that landslide hazard also relates to the existence of soil deposit (which is given in the surface geology map), past landslide events (which are compiled from "Annual Rainfall and Landslides" published by GEO), potential runout of landslides (which is estimated by aerial photograph and expert opinion), and past rainfall record (which is the average of the maximum monthly rainfall from 1990 to 2000 recorded by the Hong Kong Observatory). The last two layers deserve more elaboration. To eliminate subjective bias in estimating the potential runout of landslides, numerical model based on debris flow dynamics should be used to simulate the hazardous zone. Such analysis is, however, out of the scope of the present study. Regarding the rainfall layer, it is debatable on how to incorporate rainfall into the hazard analysis. In this study, the monthly rainfall map with the maximum value within the 11 year period from 1990 to 2000 are extracted and averaged using raster calculation to yield our rainfall hazard raster map. The hazard maps for these seven layers of parameters are shown in Fig. 15.

As shown in Table 12 of Evans et al. (1999), the correlation between elevation and landslide occurrence is not strong, thus a weighting of 0.5 is assigned to the elevation layer in Table 1. A weighting factor of 2 has been assigned to slope angle and past landslide events, since Table 8 of Evans et al. (1999) shows a very strong slope angle dependence of landslide and location with landslide history is considered to be highly susceptible to

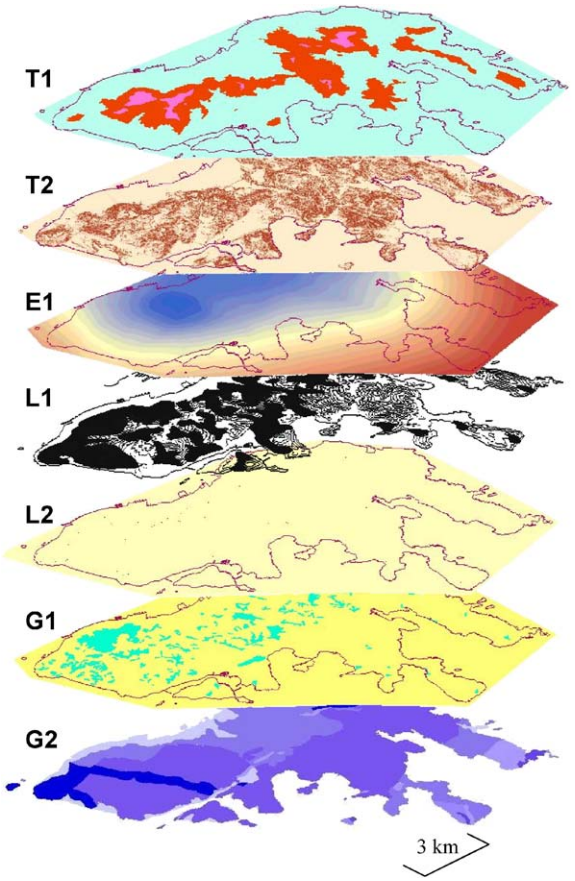

Fig. 15. Seven layers of GIS maps used in generating landslide hazard map for Hong Kong Island (from top to bottom): T1 = elevation; T2 = slope; E1 = rainfall; L1 = potential runout of landslides; L2 = landslide inventory; G1 = soil deposition; G2 = geology.

future landslides because of the local geomorphological and geological conditions. All other factors are assigned with an equal weighting of 1. As we mentioned earlier, our assigned values of W_j and H_{ji} given in Table 1 should be subject to critical review, which, however, is out of the scope of the presentation. Our main focus here is to illustrate the powerfulness of GIS in the process of hazard estimation.

The landslide hazard at each location $\boldsymbol{x}$ (denoted by pixel of 10 m × 10 m in Figs. 15 and 16) is calculated according to

$$\text{Hazard}(x) = F(x)\sum_{j=1}^{7}[W_j H_{ji}(x)]/\sum_{j=1}^{7} W_j, \tag{3}$$

where $F(\boldsymbol{x})$ is a filter function defined by

$$\begin{aligned} F(x) &= 0 \quad \text{if } \theta < 15^\circ \text{ and } H_{j25} = 0 \\ &= 1 \qquad \text{otherwise} \end{aligned}. \tag{4}$$

Since the value on the right-hand side of Eq. (3) are scaled with respect to the sum of the weightings, the maximum value of Hazard($\boldsymbol{x}$) at any pixel must be less than or equal to 1. The filter function $F(\boldsymbol{x})$ is introduced here to remove unrealistic landslide hazard on flat land which is far away from hillside. More specifically, all landslide hazards contributed from rainfall, elevation, geology will be removed if the local ground is flat and future landslides are under likely to reach this area. The hazard map calculated based upon Eqs. (3) and (4) using "raster calculator" available in ArcGIS 8.2 is shown in Fig. 16(d).

One of the beauties of using GIS is that parametric analysis can be done easily. Fig. 16 shows four hazard maps using various weightings for the seven layers of parameters. By neglecting the effect of elevation (which does not correlate strongly with landslide) and the potential runout zone (which is subject to bias), Fig. 16(a) shows the hazard map of Hong Kong Island by setting $W_1 = W_6 = 0$ with all other weightings equal 1. It appears that the most hazardous zones are mid-level and peak area. By ignoring the influence from potential runout zone, Fig. 16(b) shows a hazard map of Hong Kong Island by setting $W_6 = 0$ with all other weightings equal 1. The overall hazard distribution is somewhat similar to that of Fig. 16(a) except that hazard is more visible and evenly distributed on highlands. The hazard map given in Fig. 16(c) is based on the weightings given in Table 1 except for $W_6 = 2$, which is used to illustrate the effect of runout prediction on the overall hazard. This figure demonstrates that hazard can be more localized comparing to Fig. 16(d) if a reliable estimate of the landslide runout can be found. On the contrary, unreliable prediction on the potential runout zone can lead to misleading hazard estimation. Fig. 16 (d) shows a hazard map for the weightings shown in Table 1.

In short, GIS technology can be used effectively to combine the hazard contributions from various factors simultaneously and efficiently.

4.4. Risk analysis using raster calculation

Landslide risk can be estimated based on the following formula:

$$\text{Risk}(\boldsymbol{x}) = \text{Hazard}(\boldsymbol{x}) \times \text{Exposure}(\boldsymbol{x}), \tag{5}$$

where the Exposure($\boldsymbol{x}$) has been set to Population($\boldsymbol{x}$) in this study, which is the raster value of the population map given in Fig. 17. The population map is from the 2001 census conducted by the Census and Statistics Department of the Hong Kong SAR government. Similar to the case of hazard, the maximum value on the population map has been scaled to 1 in Fig. 17. In particular, Table 2 shows 7 classes of population and the corresponding proposed exposure index. It was discovered that the population density within each census area

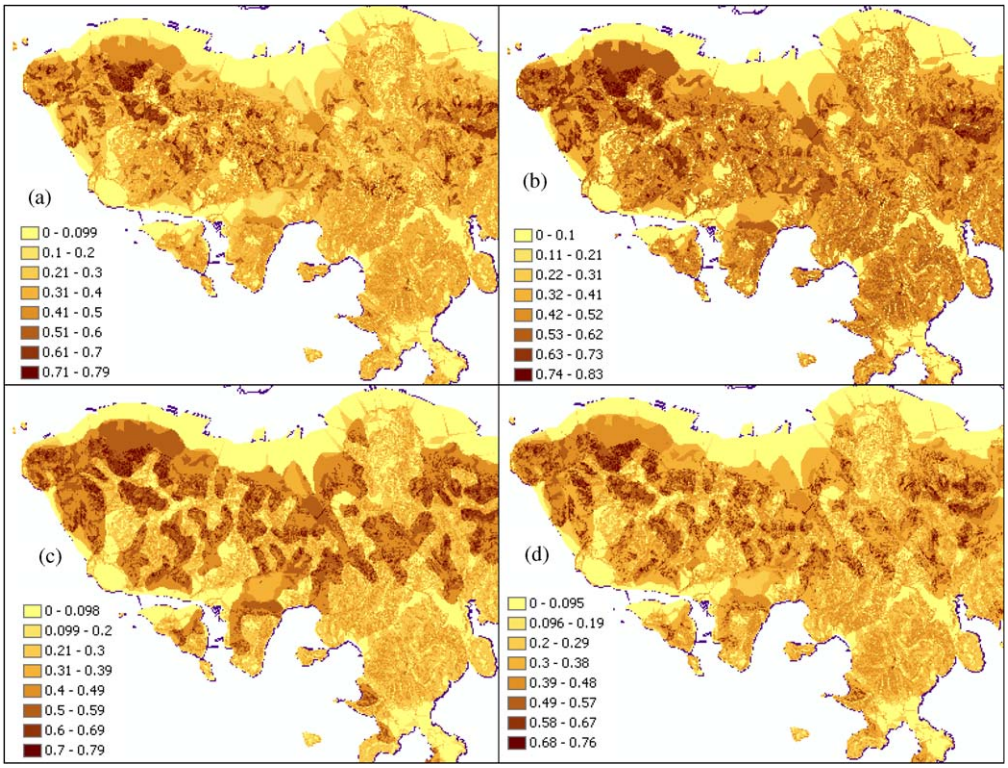

Fig. 16. Hazard map generated by layers of information from Fig. 15: (a) $W_1 = W_6 = 0$ with all other weightings equal 1; (b) $W_6 = 0$ with all other weightings equal; (c) $W_6 = 2$ with all other weightings given in Table 1; and (d) all weightings given in Table 1.

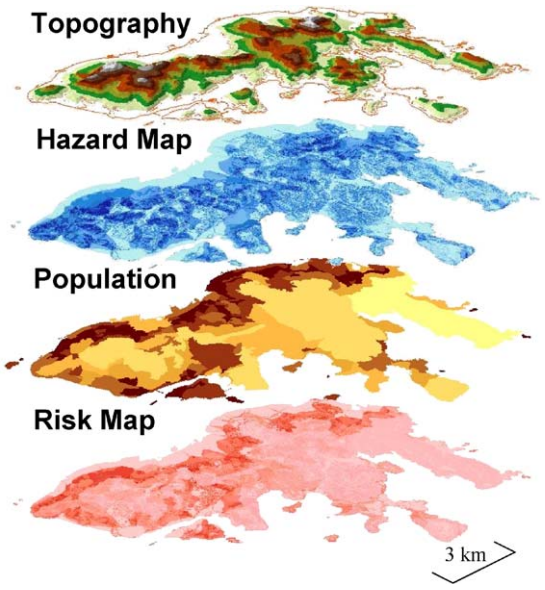

Fig. 17. Hazard map generated by layers of information from Fig. 15 together with risk map. Risk map is product of hazard map and scaled population map; and topography layer is given for reference.

Table 2
Exposure index for different population ranges used our landslide risk analysis

Class	Population (person/km^2)	Exposure index
1	<208	0.1429
2	208–982	0.2857
3	982–2087	0.4286
4	2087–4419	0.5714
5	4419–9022	0.7143
6	9022–34860	0.8571
7	$>$ 34,860	1.0000

on Hong Kong Island varies significantly. The sparsest area consists of 179 person/km^2 whilst the densest region consists of 613,725 person/km^2. And the densest areas were only found at a few locations within the urban area of the Victoria Harbour to which landslide hazard has been set to zero by the factor $F(\boldsymbol{x})$ defined in (4). Consequently, a linear scaling used for establishing the hazard index for the landslide events and rainfall cannot be applied here. The classification shown in Table 2 is made based on the criterion that the numbers of pixels

fall within each class are equal. In general, we should also consider the vulnerability of other exposures to landslides hazard, such as transportation system, buildings and public facilities. Again, the risk map shown in Fig. 17 is given for illustrative purposes only, and it is by no means conclusive.

5. Conclusion

A framework for analyzing landslide hazard analysis is proposed for Hong Kong based on landslide records through the use of GIS technology. Based on 1448 landslide data from 1984 to 1998, diurnal and seasonal distributions of landslides have been established. The cumulative fatalities and injuries caused by landslides are plotted against cumulative rainfall in Hong Kong. Total number of fatalities and injuries are 556 and 570, respectively, from 1948 to 1996. A total of 258 landslide events led to either death or injury, 117 of them killed 556 people. The average number of fatality and injury per year is 11.35 and 11.63, respectively. The annual probability of death of an individual due to landslides in Hong Kong is 2.75×10^{-6}, which is more than 10 times of the fatality rate caused by rockfall (Chau et al., 2003). It was estimated that casualty rate in Hong Kong caused by landslide is much higher than that of Italy. Strong correlation between rainfall and landslide occurrence is obtained. Considering the probability of being hit by a landslide, squatter areas on Hong Kong Island are at the highest risk. Overall, 28% of landslides land on squatter areas, 22% on road, 18% on footpath, 10% on open space, 10% on buildings, 5% on public facilities, 3% on retaining walls and drains, 3% on car-parks and the remaining 1% on vehicles. In addition, a self-similar frequency–volume relation, which is analogous to the Gutenberg–Richter relation for earthquake is established for Hong Kong Island. Using this formula, it is estimated that the return period of 26,000 m^3 landslide (the scale of 1995 Shan Wan landslide shown in Fig. 3(b)) is about 3.12 years. A landslide hazard zonation map has also been proposed based on historical data. The use of GIS technology to incorporate various layers of information is illustrated using Hong Kong Island as an example. These layers include landslide data, slope angle, elevation, lithology, soil deposit distribution, potential runout area of landslide and rainfall. In our framework, different weightings can be assigned to each layer, and unrealistic landslide hazard on lowland is eliminated by proposing a filter function. Population map is then used to illustrate the generation of landslide risk map for Hong Kong Island.

The framework of landslide hazard analysis and the potential use of GIS discussed here should provide a yardstick for further landslide hazard analysis of Hong Kong. In addition, landslide-dynamics-based numerical simulations should be included in the hazard analysis so that subjective, and potentially bias, expert opinion can be avoided. Such incorporation of landslide dynamics analysis with GIS should result in a more reliable landslide hazard map for city planning and its potential misuse can be minimized.

Acknowledgements

The work was fully supported by the Hong Kong Polytechnic University through ASD Project A226 and Infra-Faculty Project PE79 of the Faculty of Construction and Land Use. Some of the data analyses were completed in the summers of 1998 and 2002 when E.L. Fong from Northwestern University and W.Y. Wong from Cornell University were visiting Hong Kong Polytechnic University.

References

Anbalagan, R., Sharma, L., Tyagi, S., 1993. Landslide hazard zonation (LHZ) mapping of a part of Doon valley, Garhwal Himalaya, India. In: Chowdhury, R.N., Sivakumar, M. (Eds.), Environmental Management Geo-water and Engineering Aspects. Balkema, Rotterdam, pp. 253–260.

Cancelli, A., Crosta, G., 1994. Hazard and risk assessment in rockfall prone areas. In: Skipp, B.O. (Ed.), Risk and Reliability in Ground Engineering. Thomas Telford, Springfield, pp. 177–190.

Cardinali, M., Reichenbach, P., Guzzetti, F., Ardizzone, F., Antonini, G., Galli, M., Cacciano, M., Castellani, M., Salvati, P., 2002. A geomorphological approach to the estimation of landslide hazards and risks in Umbria, Central Italy. Natural Hazards and Earth System Sciences 2 (1/2), 57–72.

Carrara, A., Cardinali, M., Detti, R., Guzzetti, F., Pasqui, V., Reichenbach, P., 1991. GIS techniques and statistical-models in evaluating landslide hazard. Earth Surface Processes 16 (5), 427–445.

Carrara, A., Guzzetti, F., Cardinali, M., Reichenbach, P., 1999. Use of GIS technology in the prediction and monitoring of landslide hazard. Natural Hazards 20 (2-3), 117–135.

Chau, K.T., Wong, R.H.C., Lee, C.F., 1998. Rockfall problems in Hong Kong and some new experimental results for coefficient of restitution. International Journal of Rock Mechanics and Mining Science 35 (4–5), 662–663 (Paper No. 007).

Chau, K.T., Wong, R.H.C., Lui, J., Lee, C.F., 2003. Rockfall hazard analysis for Hong Kong based on rockfall inventory. Rock Mechanics and Rock Engineering 36 (5), 383–408.

Collison, A., Wade, S., Griffiths, J., Dehn, M., 2000. Modelling the impact of predicted climate change on landslide frequency and magnitude in SE England. Engineering Geology 55 (3), 205–218.

Coppock, J.T., 1995. GIS and natural hazards: an overview from a GIS perspective. In: Carrara, A., Guzzetti, F. (Eds.),

Geographical Information Systems in Assessing Natural Hazards. Kluwer, Dordrecht, pp. 21–34.

Dai, F.C., Lee, C.F., 2001a. Frequency–volume relation and prediction of rainfall-induced landslides. Engineering Geology 59 (3-4), 253–266.

Dai, F.C., Lee, C.F., 2001b. Terrain-based mapping of landslide susceptibility using a geographical information system: a case study. Canadian Geotechnical Journal 38 (5), 911–923.

Dai, F.C., Lee, C.F., 2002a. Landslide characteristics and, slope instability modeling using GIS, Lantau Island, Hong Kong. Geomorphology 42 (3-4), 213–228.

Dai, F.C., Lee, C.F., 2002b. Landslides on natural terrain - physical characteristics and susceptibility mapping in Hong Kong. Mountain Research and Development 22 (1), 40–47.

Dai, F.C., Lee, C.F., Li, J., Xu, Z.W., 2001. Assessment of landslide susceptibility on the natural terrain of Lantau Island, Hong Kong. Environmental Geology 40 (3), 381–391.

Dai, F.C., Lee, C.F., Ngai, Y.Y., 2002. Landslide risk assessment and management: an overview. Engineering Geology 64 (1), 65–87.

Davis, T.J., Keller, C.P., 1997. Modelling and visualizing multiple spatial uncertainties. Computers & Geosciences 23 (4), 397–408.

Dhakal, A.S., Amada, T., Aniya, M., 1999. Landslide hazard mapping and the application of GIS in the Kulekhani watershed, Nepal. Mountain Research and Development 19 (1), 3–16.

Dhakal, A.S., Amada, T., Aniya, M., 2000. Landslide hazard mapping and its evaluation using GIS: an investigation of sampling schemes for a grid-cell based quantitative method. Photogrammetric Engineering Remote Sensing 66 (8), 981–989.

Dikau, R., Cavallin, A., Jager, S., 1996. Databases and GIS for landslide research in Europe. Geomorphology 15 (3-4), 227–239.

Duarte, R.M., Marquinez, J., 2002. The influence of environmental and lithogic factors on rockfall at a regional scale: an evaluation using GIS. Geomorphology 43 (1–2), 117–136.

Einstein, H.H., 1988. Landslide risk assessment procedure. In: Landslides, 5th International Symposium on Landslides, Vol. 2. Balkema, Rotterdam, pp. 1075–1090.

Einstein, H.H., 1997. Landslide risk-Systematic approaches to assessment. In: Cruden, Fell, (Eds.), Landslide Risk Assessment. Balkema, Rotterdam, pp. 25–50.

Evans, N.C., Huang, S.W., King, J.P., 1999. The natural terrain landslide study phases I and II. GEO Report No. 73, GEO, CED, Hong Kong SAR Government, 128pp.

Fell, R., Hartford, D., 1997. Landslide risk management. In: Cruden, D.M., Fell, R. (Eds.), Landslide Risk Assessment. Balkema, Rotterdam, pp. 51–109.

Fyfe, J.A., Shaw, R., Campbell, S.D.G., Lai, K.W., Kirk, P.A., 2000. The Quaternary Geology of Hong Kong. Geotechnical Engineering Office, Hong Kong, 210pp.

Geotechnical Engineering Office (GEO), 1996. Compilation of a database on landslide Consequence. Submitted by Mitchell, McFarlane, Brentnall & Partners Int. Ltd., Agreement No. GEO 8/95, Final Report for Special Project Division, GEO, 310pp.

Gritzner, M.L., Marcus, W.A., Aspinall, R., Custer, S.G., 2001. Assessing landslide potential using GIS, soil wetness modeling and topographic attributes, Payette River, Idaho. Geomorphology 37 (1–2), 149–165.

Gupta, R.P., Joshi, B.C., 1990. Landslide hazard zoning using the GIS approach—a case-study from the Ramganga Catchment, Himalayas. Engineering Geology 28 (1–2), 119–131.

Guzzetti, F., 2000. Landslide fatalities and the evaluation of landslide risk in Italy. Engineering Geology 58 (2), 89–107.

Guzzetti, F., Carrara, A., Cardinali, M., Reichenbach, P., 1999. Landslide hazard evaluation: a review of current techniques and their application in a multi-scale study, central Italy. Geomorphology 31 (1–4), 181–216.

Hansen, A., 1984. Landslide hazard analysis. In: Brunsden, D., Prior, D.B. (Eds.), Slope Instability. Wiley, New York, pp. 523–602.

Hungr, O., 1997. Some methods of landslides hazard intensity mapping. In: Cruden, Fell, R. (Eds.), Landslide Risk Assessment. Balkema, Rotterdam, pp. 215–226.

Husein, A.I., Saleh, B., Al-Sheriadeh, M.S., Hamza, M.S., 2000. Mapping of landslide hazard zones in Jordan using remote sensing and GIS. Journal of Urban Planning and Development ASCE 126 (1), 1–17.

Jibson, R.W., Harp, E.L., Michael, J.A., 2000. A method for producing digital probabilistic seismic landslide hazard maps. Engineering Geology 58 (3–4), 271–289.

Kienholz, H., 1978. Maps of geomorphology and natural hazards of Grindelwald, Switzerland: scale 1:10,000. Arctic and Alpine Research 10 (2), 169–184.

Lazzari, M., Salvaneschi, P., 1999. Embedding a geographic information system in a decision support system for landslide hazard monitoring. Natural Hazards 20 (2–3), 185–195.

Lee, C.F., Ye, H., Yeung, M.R., Shan, X., Chen, G., 2001. AIGIS-based methodology for natural terrain landslide susceptibility mapping in Hong Kong. Episodes 24 (3), 150–159.

Lee, S., Min, K., 2001. Statistical analysis of landslide susceptibility at Yongin, Korea. Environmental Geology 40 (9), 1095–1113.

Leroi, E., 1997. Landslide Risk Mapping: Problems, Limitation and Developments. In: Cruden, Fell, (Eds.), Landslide Risk Assessment. Balkema, Rotterdam, pp. 239–250.

Luzi, L., Pergalani, F., 1996. Applications of statistical and GIS techniques to slope instability zonation (1:50.000 Fabriano geological map sheet). Soil Dynamics and Earthquake Engineering 15 (2), 83–94.

Luzi, L., Pergalani, F., Terlien, M.T.J., 2000. Slope vulnerability to earthquakes at subregional scale, using probabilistic techniques and geographic information systems. Engineering Geology 58 (3–4), 313–336.

Mejianavarro, M., Wohl, E.E., Oaks, S.D., 1994. Geological hazards, vulnerability, and risk assessment using GIS-model for Glenwood-Springs, Colorado. Geomorphology 10 (1–4), 331–354.

Miles, S.B., Ho, C.L., 1999. Rigorous landslide hazard zonation using Newmark's method and stochastic ground motion simulation. Soil Dynamics Earthquake Engineering 18 (4), 305–323.

Miles, S.B., Keefer, D.K., 1999. Evaluation of seismic slope-performance models using a regional case study. Environmental & Engineering Geoscience 6 (1), 25–39.

Miller, D.J., Sias, J., 1998. Deciphering large landslides: linking hydrological, groundwater and slope stability models through GIS. Hydrological Processes 12 (6), 923–941.

Nagarajan, R., Mukherjee, A., Roy, A., Khire, M.V., 1998. Temporal remote sensing data and GIS application in landslide hazard zonation of part of Western Ghat, India. International Journal of Remote Sensing 19 (4), 573–585.

PIARC-World Road Association, 1997. Landslides-techniques for evaluating hazard. PIARC Technical Committee on Earthworks, Drainage, Subgrade (C12), pp. 1–117.

Refice, A., Capolongo, D., 2002. Probabilistic modeling of uncertainties in earthquake-induced landslide hazard assessment. Computers & Geosciences 28 (6), 735–749.

Rowbotham, D.N., Dudycha, D., 1998. GIS modelling of slope stability in Phewa Tal watershed, Nepal. Geomorphology 26 (1–3), 151–170.

Saha, A.K., Gupta, R.P., Arora, M.K., 2002. GIS-based landslide hazard zonation in the Bhagirathi (Ganga) Valley, Himalayas. International Journal of Remote Sensing 23 (2), 357–369.

Scholz, C., 1990. The Mechanics of Earthquakes and Faulting. Cambridge University Press, Cambridge, 439pp.

Temesgen, B., Mohammed, M.U., Korme, T., 2001. Natural hazard assessment using GIS and remote sensing methods, with particular reference to the landslides in the Wondogenet area, Ethiopia. Physics and Chemistry of the Earth, Part C 26 (9), 665–675.

van Westen, C.J., 2000. The modelling of landslide hazards using GIS. Surveys in Geophysics 21 (2–3), 241–255.

van Westen, C.J., Terlien, M.T.J., 1996. An approach towards deterministic landslide hazard analysis in GIS. A case study from Manizales (Colombia). Earth Surface Processes 21 (9), 853–868.

van Westen, C.J., Seijmonsbergen, A.C., Mantovani, F., 1999. Comparing landslide hazard maps. Natural Hazards 20 (2–3), 137–158.

Varnes, D.J., 1984. Landslide hazard zonation: a review of principles and practice. UNESCO, France, pp. 1–63.